Polymer 50 (2009) 2472–2480

Contents lists available at ScienceDirect

Polymer

journal homepage: www.elsevier.com/locate/polymer

Preparation and characterization of thermoplastic olefin/nanosilica composites using a silane-grafted polypropylene matrix

Mathieu Bailly, Marianna Kontopoulou*

Department of Chemical Engineering, Queen's University, Kingston, ON, Canada K7L 3N6

ARTICLE INFO

Article history:
Received 21 January 2009
Received in revised form
20 March 2009
Accepted 20 March 2009
Available online 27 March 2009

Keywords:
Nanocomposites
Thermoplastic olefins
Silane-grafted polypropylene

ABSTRACT

This work reports the morphology and physical properties of silane-grafted polypropylene (PP-g-VTEOS) reinforced with silica nanoparticles and toughened with an elastomeric ethylene–octene copolymer (POE). Vinyltriethoxysilane (VTEOS) was grafted to polypropylene (PP) to form (PP-g-VTEOS), using a peroxide-initiated melt compounding technique. TEM observations of composites containing up to 7 wt% of the nanosilica revealed good dispersion of the silica nanoparticles, which partitioned selectively within the PP-g-VTEOS matrix. Rheological characterization in the linear viscoelasticity region showed significant increases in the low-frequency complex viscosity, storage and loss moduli, which stem from the polymer/filler and filler/filler interactions. The effects of surface treatment of the nanosilica on the morphology, thermal and mechanical properties of the composites were also investigated. The mechanical properties of the composites were greatly enhanced in terms of tensile and flexural strength, while impact strength was preserved when the silane-treated nanosilica was used.

1. Introduction

Isotactic polypropylene (PP) is a commodity polymer with widespread applications due to its good mechanical and thermal properties, as well as low cost. To improve its ductility and toughness, impact modifiers like ethylene–propylene–diene (EPDM), ethylene–propylene rubber (EPR) and various other polyolefinic elastomers (POEs) are commonly used [1–5]. A fine dispersion of the rubber particles is required to achieve good ductile properties and an overall balanced performance in all PP/elastomer compounds, also known as thermoplastic olefin blends (TPOs).

Inorganic fillers such as talc, silica, $CaCO_3$, $BaSO_4$ and $Mg(OH)_2$ are used as reinforcing agents in these PP/rubber blends. In their presence the tensile strength, Young's and flexural moduli improve substantially, usually at the expense of the elongation at break [6–8]. During the last decade there has been great interest in PP-based nanocomposite blends that contain finely dispersed nanofillers, such as exfoliated or intercalated nanoclays [9], nano$CaCO_3$ [10] and nanosilica [11–14].

Due to the nonpolar character of the PP, functionalization of the polymer matrix and/or treatment of the nanoparticles are needed to achieve a good dispersion of the rigid nanoparticles and satisfactory mechanical properties. This can be achieved via different routes, such as functionalization of the PP matrix with maleic anhydride [15] or silanes [16–18], addition of a compatibilizer [7,12,19], or chemical treatment of the nanoparticles [20]. In the case of silica the latter may be accomplished through grafting macromolecules directly onto the nanoparticles [21,22] or by using coupling or coating agents [23–30].

In our previous work, where we added nanosilica to reinforce TPOs using maleated PP as a compatibilizer, we showed that optimum benefits can be obtained when the filler is selectively localized within the PP matrix [12,13]. In the present work we functionalized PP by peroxide-initiated grafting of vinyltriethoxysilane, to obtain a PP-g-VTEOS derivative. The alkoxysilane functionality can engage the hydroxyl groups on the surface of silica to provide covalent bonds between the polymer and the filler, resulting in improved compatibility between the matrix and the filler. The morphology as well as the mechanical, thermal and rheological properties of the nanocomposites is presented with a particular focus on the matrix/filler interactions.

2. Experimental

2.1. Materials

Polypropylene, Escorene PP1042, MFR 1.9 g/10 min at 230 °C, was supplied by ExxonMobil Chemical. Ethylene–octene copolymer polyolefin elastomer POE, Engage 8130, MFR 1.0 g/10 min at 190 °C, from Dow Chemical was used as an impact modifier.

* Corresponding author. Tel.: +1 613 533 3079; fax: +1 613 533 6637.
E-mail address: marianna.kontopoulou@chee.queensu.ca (M. Kontopoulou).

0032-3861/$ – see front matter © 2009 Elsevier Ltd. All rights reserved.
doi:10.1016/j.polymer.2009.03.034

Vinyltriethoxysilane (VTEOS, 97%, Aldrich Chemical Company Inc.) and dicumyl peroxide (DCP, 98%, Sigma Aldrich) were used as received. Irganox 225 antioxidant was obtained from Ciba-Geigy.

2.2. Characterization of nanofillers

Three different types of silica, supplied by Evonik Industries (formerly Degussa Corp.) were used. A hydrophilic fumed silica Aerosil® 200 with an average particle size of 12 nm and a specific surface area (SSA) of 200 ± 25 m^2/g, and two hydrophobic surface modified nanosilicas: Aerosil® R805 modified with octylsilane (oct-SiO_2) having an SSA of 150 ± 25 m^2/g and Aerosil® R816 modified with hexadecylsilane (hex-SiO_2) having an SSA of 190 ± 20 m^2/g.

The relative degree of modification with silanes was examined by thermogravimetric analysis (TGA) and FT-IR. TGA was performed using a TA Instruments Q500 series thermogravimetric analyzer. Samples were heated from room temperature to 900 °C at a rate of 10 °C/min under nitrogen atmosphere. Oct-SiO_2 exhibited the highest amount of weight loss; 7 wt% compared to SiO_2 and hex-SiO_2 which showed a weight loss of 1.5 and 2.3 wt% respectively.

From the FT-IR spectra the area of the peak corresponding to the –OH groups in the 2700–3800 cm^{-1} range was compared relative to the area of a reference peak at 1650 cm^{-1}. It was found that oct-SiO_2 is more heavily modified than hex-SiO_2 since the area under its peak is lower, indicating that more hydroxyl groups have been substituted by silane groups.

2.3. Grafting procedure and nanocomposites preparation

PP powder (40 g) was tumble-mixed with a solution of DCP (0.1 wt%) in VTEOS (5 wt%) for 20 min. The grafting reaction was carried out in a Haake PolyLab rheometer equipped with a Rheomix 610p mixing chamber and roller rotors. The rotation speed, temperature and residence time were fixed at 60 rpm, 190 °C and 8 min respectively. 0.2 wt% of antioxidant was added after 3 min of mixing time. The grafting reaction of VTEOS onto PP, giving PP-g-VTEOS, has been described in detail by Parent et al. [31]. Following the formation of PP-g-VTEOS, various amounts of nanosilica, ranging from 2 to 7 wt% were added and mixed for 2 min, followed by the introduction of 20 wt% POE, which was compounded for 3 min.

In order to obtain a non-functionalized PP sample suitable for comparison with the VTEOS grafted material, PP was reacted with 0.1 wt% DCP for 3 min to obtain a degraded derivative (deg-PP). Subsequently 0.2 wt% of antioxidant was added; the total mixing time was 8 min. This procedure provided a sample with comparable rheological properties, as well as similar heat history as the PP-g-VTEOS.

2.4. Characterization of functionalized PP

PP-g-VTEOS samples for graft content analysis were purified from residual VTEOS by dissolving in hot refluxing xylene, precipitating from acetone, and drying under vacuum at 60 °C. FT-IR spectra were obtained using a Nicolet Avatar 360 FTIR ESP instrument. Grafted VTEOS contents were calculated from FT-IR integrations of the 1064–1094 cm^{-1} absorbance of the silane relative to a 422–496 cm^{-1} internal standard region originating from PP. A calibration curve for the determination of the graft content was obtained by using known mixtures of PP and an unreactive silane (ethyltriethoxysilane) as standards. Based on this calculation the grafted VTEOS content was determined to be 0.45 wt%.

2.5. Microscopy

The state of dispersion of the filler was assessed by TEM imaging, using an FEI Tecnai 20 instrument. Ultra-thin sections were cryomicrotomed using a Leica ultra microtome and stained in RuO_4 vapour to enhance the phase contrast between the PP and elastomer phases.

Samples were prepared for SEM observations, by compression molding using a Carver press at 190 °C, and 10 MPa for 1 min, then freeze fractured in liquid nitrogen. The elastomer phase was etched in toluene for 2 h at 80 °C. The etched surfaces were observed on a JEOL JSM-840 scanning electron microscope. The SEM images were analyzed by using the Sigma Scan Pro image analysis software to estimate the average diameters of the dispersed elastomer phase. Between 200 and 800 particles were analyzed per sample. The diameter of each particle (D) was calculated using its area determined by the image analysis software. The number (D_n) and volume (D_v) diameters were calculated with the following formulae:

$$D = \sqrt{\frac{4\mathrm{Area}}{\pi}}, \quad D_n = \frac{\sum n_i D_i}{\sum n_i}, \quad D_v = \frac{\sum n_i D_i^4}{\sum n_i D_i^3} \tag{1}$$

n_i being the number of particles having a diameter of D_i.

Finally, the polydispersity index was calculated as:

$$\mathrm{PI} = \frac{D_v}{D_n} \tag{2}$$

2.6. Mechanical properties

Tensile properties were measured using an Instron 3369 universal tester, at crosshead speeds of 10 mm/min. Dog-bone shaped specimens were cut with a Type V die according to ASTM D638 from 1.5 mm thick sheets, which were prepared by compression molding of the compounded samples at approximately 200 °C using a Carver press.

Flexural tests were performed according to ASTM D790, procedure B, at a speed of 13.65 mm/min. Rectangular bars of dimensions $127 \times 12.7 \times 3.2$ mm were produced by compression molding at 200 °C. Notched Izod impact tests were carried out on an Instron BLI impact tester at room temperature according to ASTM D 256. Specimens of dimensions $64 \times 12.7 \times 3.2$ mm were prepared by compression molding at 200 °C. At least 5 specimens were tested for each sample and the average value is reported.

2.7. Thermal properties

The melting and crystallization temperatures, as well as heats of fusion and crystallization of the samples were measured on a TA Q100 Differential Scanning Calorimeter (DSC). The samples were first heated to 200 °C for 5 min to eliminate their thermal history and subsequently cooled to −40 °C at a rate of 5 °C/min. The second endotherm was recorded by heating at 5 °C/min. The heat of crystallization was calculated relevant to that of pure crystalline PP (191.4 J/g according to [32]).

2.8. Rheological characterization

Rheological characterization was carried out on a Reologica ViscoTech oscillatory rheometer using 20 mm parallel plate fixtures, with a gap of 1 mm at 200 °C, under nitrogen blanket. The rheometer was operated in the dynamic oscillatory mode in the linear viscoelasticity region – i.e. with strain under 10%, which was determined by stress sweep experiments. The elastic modulus (G'),

loss modulus (G'') and complex viscosity (η^*) were measured as functions of the angular frequency (ω).

3. Results

3.1. Effect of VTEOS grafting on rheological properties

The chemical treatment of PP with peroxides unavoidably results to degradation via chain scission, lowering substantially the viscosity of the material. This is clearly seen in Fig. 1, which shows the complex viscosity of PP prior and after chemical modification. On the other hand, the presence of VTEOS grafts does not have a significant effect on the rheology of the materials, as seen through the comparison of the deg-PP and PP-g-VTEOS. Based on the viscosities of both PP-g-VTEOS and deg-PP used in the TPO compounds, a suitable polyolefin elastomer with a comparable viscosity was chosen, to provide an optimal viscosity ratio at shear rates between 20 and 100 s^{-1}, which are relevant to compounding with the batch mixer.

3.2. Morphology

The properties of ternary nanocomposites are largely determined by the localization and the state of dispersion of the inorganic fillers, as well as the size and the distribution of the dispersed polymer phase. Various morphologies, depending on the location of the filler, may be obtained by changing the mixing procedure. Morphologies such as a separate dispersion structure, where the filler resides in the matrix, encapsulation/core–shell structure, where the filler partitions preferentially in the dispersed phase, and mixtures of the former two, have been reported. It has been demonstrated that better mechanical properties are achieved when the inorganic fillers are localized within the matrix [12,13]. In this work, adding the silica prior to the addition of the elastomeric phase resulted in a separated microstructure, where the silica nanoparticles remain exclusively in the PP matrix, irrespective of filler treatment (Fig. 2).

The state of dispersion of the filler depends on the silica treatment and the presence of matrix functionality: It is well-known that the silanol groups present at the surface of the silica nanoparticles tend to form hydrogen bonds, resulting in a strong tendency toward agglomeration during melt compounding. This is evident in the deg-PP/POE/SiO_2 composites containing untreated SiO_2 and a non-functionalized matrix (Fig. 2(a)). Given the large size of the aggregates (about 1 μm), these compounds can rather be characterized as "macrocomposites". Introduction of the alkoxysilane functionality results in the establishment of covalent bonding between the polymer and the filler, by engaging the hydroxyl groups on the surface of the silica, according to Scheme 1. This improves the stress transfer to the filler during melt compounding, resulting in more efficient breakup of the filler aggregates, as evidenced in the PP-g-VTEOS/POE/SiO_2 composites of Fig. 2(b). Further, replacing silanol groups located at the surface of the nanoparticles by silane groups consisting of long alkyl chains will tend to reduce the size of the aggregates, by breaking up the hydrogen bonds between the particles, therefore improving the dispersion of the fillers, as seen on the TEM images of PP-g-VTEOS/POE reinforced with oct-SiO_2 and hex-SiO_2 (Fig. 2(c)–(e)). Additionally, the surface treatment of the nanoparticles renders the nanoparticles more hydrophobic owing to the presence of the long alkyl chains in the grafted silane groups, therefore reducing their polar nature. This further contributed to the improved dispersion of the modified silica. Surface treatment of the nanoparticles provided a very efficient means for their good dispersion, irrespective of presence of functionality in the matrix, as shown by the relatively good dispersion of oct-SiO_2 in the non-functionalized deg-PP matrix (Fig. 2(d)).

Hex-SiO_2 contains longer alkyl chains, which would result in a reduced tendency of the filler to agglomerate, because of steric hindrance [33]. However, comparison of the two silane modified silicas by TGA and FT-IR spectroscopy showed that oct-SiO_2 particles are more heavily modified than hex-SiO_2 particles. This is probably the reason why oct-SiO_2 composites exhibit improved dispersion (Fig. 2(c) vs. (e)), although additional research is needed to differentiate between these factors.

In addition to the differences in filler dispersion seen by TEM, SEM observations revealed variabilities in the size of the dispersed elastomer phase. In Fig. 3, which shows the SEM images of the PP-g-VTEOS/POE and PP-g-VTEOS/POE/7 wt% oct-SiO_2, it can be seen that in the presence of the filler the size of the dispersed phase becomes significantly finer. The results of the image analysis performed on the SEM images of PP-g-VTEOS/POE blends containing up to 7 wt% of oct-SiO_2 are presented in Fig. 4 and confirm a shift in size in favour of finer particles, at the highest nanosilica content. The number and volume average particle diameters for all the composites are summarized in Table 1.

Theories that describe the reduction of the size of the dispersed phase in the presence of nanoparticles vary, depending on whether the filler is located in the continuous phase, in the dispersed phase, or at the interphase between the two blend components. Compatibilizing effects due to polymer adsorption on the filler surface, as well as reduction in the interfacial tension between the two phases in the presence of the filler are the generally accepted mechanisms when the filler is located at the interface [11,34,35]. However these mechanisms are obviously not dominant when the filler resides in the matrix [36]. In that case the most likely explanations include the possibility that exfoliated clay platelets or well dispersed nanoparticles may hinder particle coalescence by acting as physical barriers [9,37]. Furthermore it has been suggested that an immobilized layer, consisting of the inorganic nanoparticles and bound polymer forms around the droplets of the dispersed phase [38]. The reduced mobility of the confined polymer chains that are bound to the filler likely causes a decrease in the drainage rate of the thin film separating two droplets [36,39]. If this is the case, this phenomenon would be dependent on filler concentration; presumably higher filler concentrations would be needed to obtain the same effect in

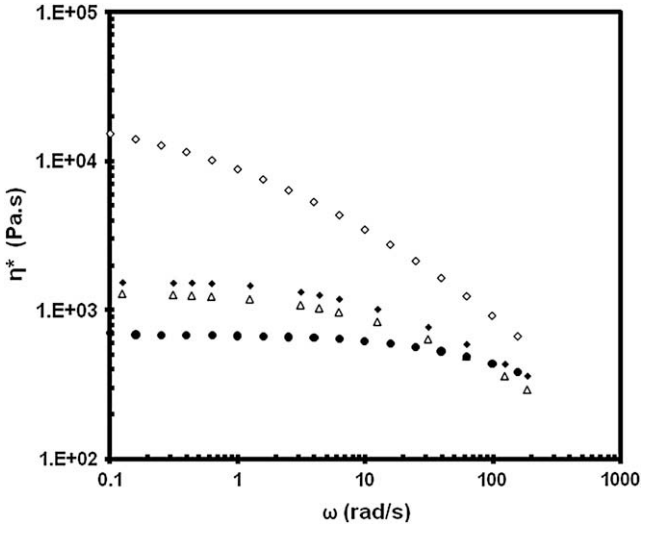

Fig. 1. Complex viscosity as a function of frequency, obtained by dynamic oscillatory experiments at 200 °C. Symbols are (◇) PP; (△) PP-g-VTEOS; (●) POE; (◆) deg-PP.

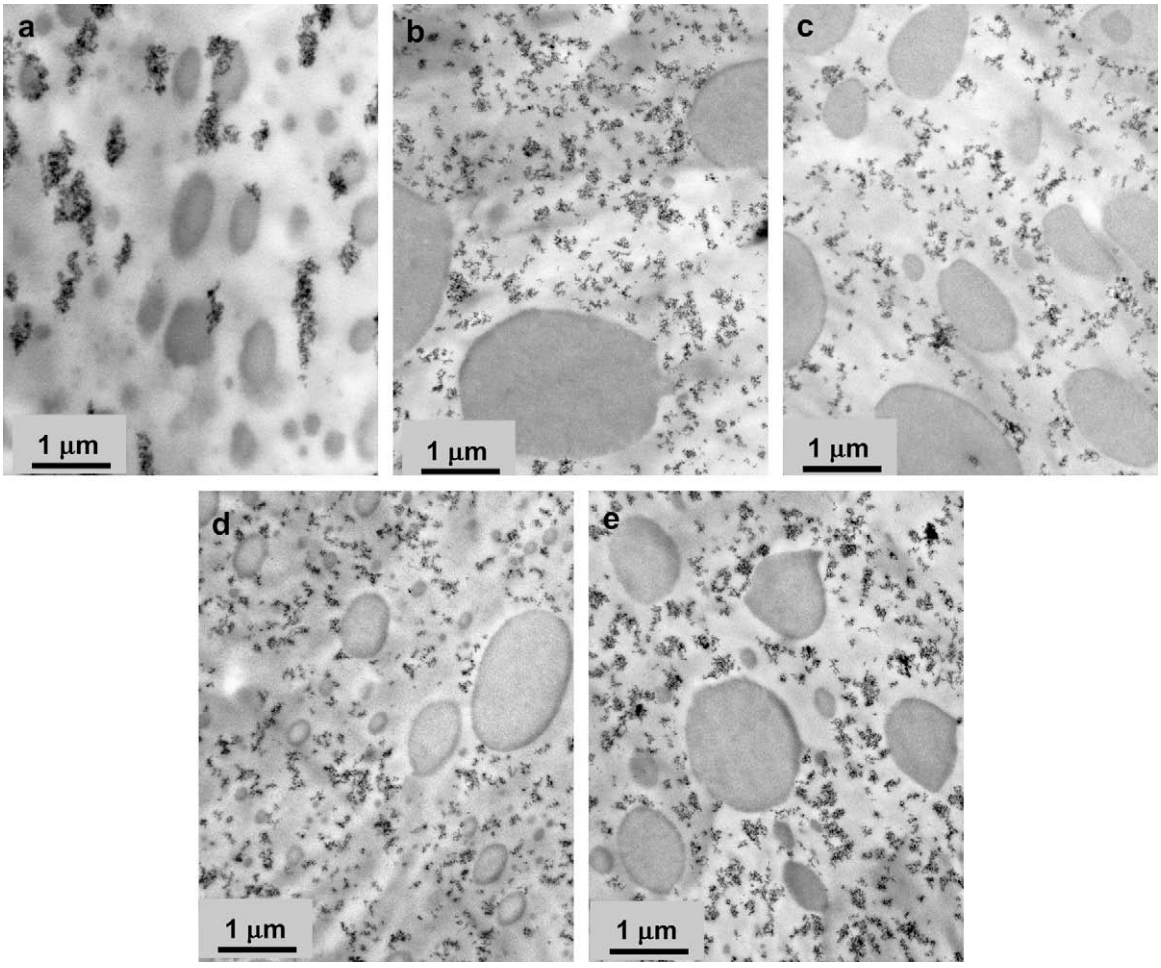

Fig. 2. TEM images of (a) deg-PP/POE/SiO_2; (b) PP-g-VTEOS/POE/SiO_2; (c) PP-g-VTEOS/POE/oct-SiO_2; (d) deg-PP/POE/oct-SiO_2; and (e) PP-g-VTEOS/POE/hex-SiO_2. Silica content is 5 wt%. The darker domains correspond to the POE dispersed phase.

the case of low aspect fillers, such as nanosilica. This is consistent with our observations, which show that a reduction in size is only obtained above a certain nanosilica content.

3.3. Rheological characterization

As shown from the oscillatory shear results in Figs. 5 and 6 the composites exhibit loss of the Newtonian plateau and higher values of the complex viscosity and moduli as the filler content increases above 2 wt%. The disappearance of the terminal flow region and appearance of a yield stress become more pronounced at higher filler loadings (Fig. 5). The appearance of yielding at 7 wt% is consistent with the existence of a "percolation" threshold. This behaviour has been attributed to the formation of a "polymer/filler" network [40]. These trends are better reflected by the loss tangent vs. frequency data, as shown in Fig. 5(c). First of all the secondary relaxation, attributable to the presence of a dispersed deformable phase [41] can be clearly seen in the curves corresponding to the PP-g-VTEOS/POE blend; addition of just 2 wt% oct-SiO_2 does not appear to affect this response. Both samples tend to reach terminal flow eventually. Significant deviations from the terminal flow are noted however as the oct-SiO_2 content increases further, with the

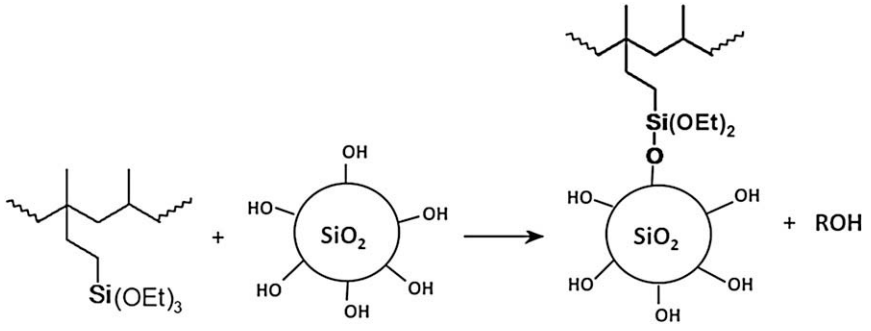

Scheme 1. Schematic illustration of the hydrolysis reaction between the silanol groups located at the surface of the silica with the VTEOS grafts.

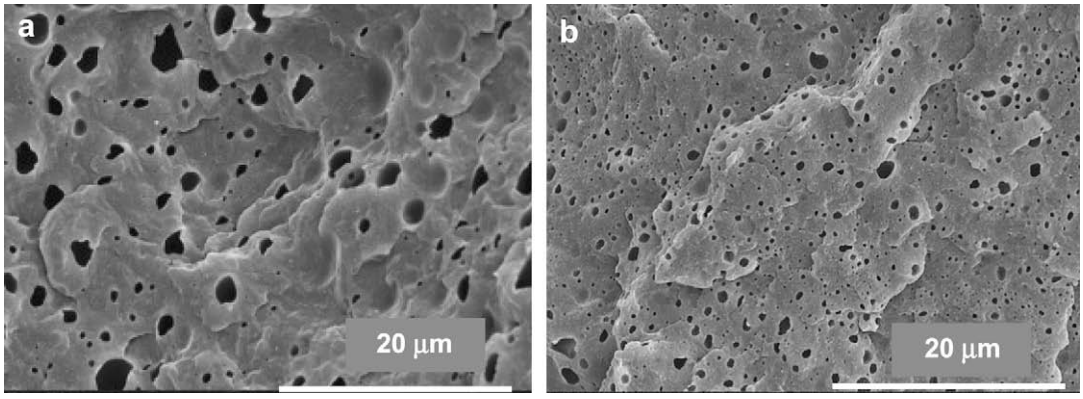

Fig. 3. SEM micrographs of (a) PP-g-VTEOS/POE; (b) PP-g-VTEOS/POE/oct-SiO_2 7-wt%. The holes correspond to the etched dispersed phase.

highest content approaching what seems like a "secondary" plateau.

Whereas the rheological response is dependent on silica content, silica treatment and matrix functionalization also play a significant role, as shown in Fig. 6. Our results show two distinctly different trends. On the one hand, the presence of large aggregates, evident in the deg-PP/POE/SiO_2 composites (see also Fig. 2(a)) results in a substantial increase in viscosity and elasticity over the entire frequency range. Such behaviour is typical when filler/filler interactions due to the presence of hydrogen bonding are predominant [27,40]. Addition of the alkoxysilane functionality introduced covalent bonding and improved the dispersion of the filler considerably, resulting in a nanocomposite as shown in Fig. 2(b). The complex viscosity and elasticity appear substantially lower compared to deg-PP/POE/SiO_2; still there is a significant increase compared to the base material. The extent of modification of the silica particles further seems to influence the low-frequency properties, with the more heavily modified oct-SiO_2 displaying the most pronounced increase. These results imply that the rheological properties depend on both the state of dispersion of the fillers and the presence of chemical bonding. PP-g-VTEOS/POE/oct-SiO_2 exhibits the largest enhancement in rheological properties compared to all the other composites containing PP-g-VTEOS, presumably because it combines the fine dispersion of the particles with the formation of covalent bonds, thus establishing the strongest polymer/filler interactions.

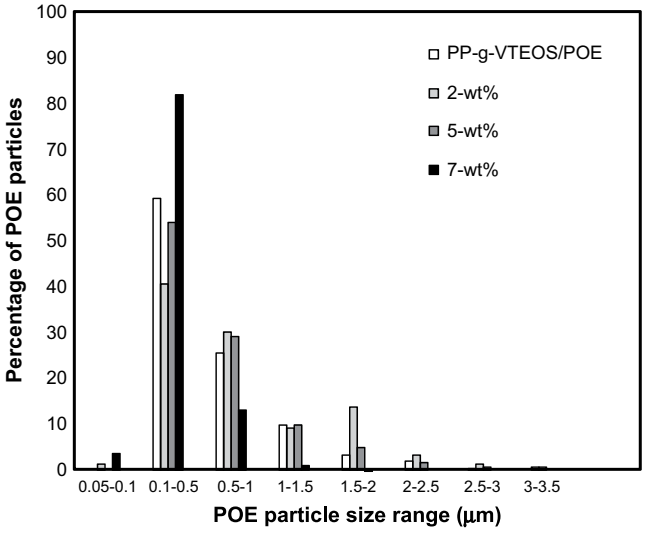

Fig. 4. POE particle size distribution in PP-g-VTEOS/POE/oct-SiO_2 composites at different silica contents.

3.4. Thermal properties

The results of the thermal characterization of the composites by DSC are shown in Table 2. Once again surface treatment and aggregation seem to be of prime importance: The unmodified SiO_2 particles, which have the highest specific surface area (SSA) have a pronounced nucleation effect, increasing the crystallization temperature by about 10 °C, followed by hex-SiO_2, while the most heavily modified oct-SiO_2, which has the lowest SSA, has the least effect on crystallization temperature. The overall crystallinity of the composites follows a similar trend. It is worth noting that the nucleation effect is absent in the case of the macrocomposite deg-PP/POE/SiO_2, obviously because of the substantially reduced surface area available for nucleation in the presence of large aggregates, hindering the ability of the particles to act as efficient nucleating agents.

3.5. Mechanical properties

As shown in Table 3, the addition of POE decreases the tensile strength and Young's modulus of the PP matrix and enhances the elongation at break and impact strength, resulting in a more ductile material. This is a well-known consequence of elastomer addition [3,4] and confirms the ability of POE to act as an efficient impact modifier for the PP-g-VTEOS matrix.

Significant reinforcement was achieved upon silica addition. The dispersion of the nanoparticles plays a determinant role in the ability of the rigid nanofillers to carry the applied load. A fine dispersion is accompanied by a larger interfacial area and a strong adhesion between the fillers and the matrix; this is the basis of an

Table 1
Particle sizes for composites containing various amounts and types of nanosilica, obtained through image analysis of SEM images.

Sample	Number average diameter D_n (μm)	Volume average diameter D_v (μm)	Polydispersity index
PP-g-VTEOS/POE	0.58 ± 0.50	2.25	3.68
PP-g-VTEOS/POE/oct-SiO_2 2%	0.81 ± 0.62	2.04	2.45
PP-g-VTEOS/POE/oct-SiO_2 5%	0.64 ± 0.50	2.42	3.71
PP-g-VTEOS/POE/oct-SiO_2 7%	0.30 ± 0.21	0.82	2.27
PP-g-VTEOS/POE/SiO_2 5%	0.91 ± 0.70	2.93	3.06
PP-g-VTEOS/POE/hex-SiO_2 5%	0.64 ± 0.65	2.98	4.22
Deg-PP/POE/oct-SiO_2 5%	0.60 ± 0.73	2.97	4.46
Deg-PP/POE/SiO_2 5%	0.44 ± 0.26	2.09	1.93

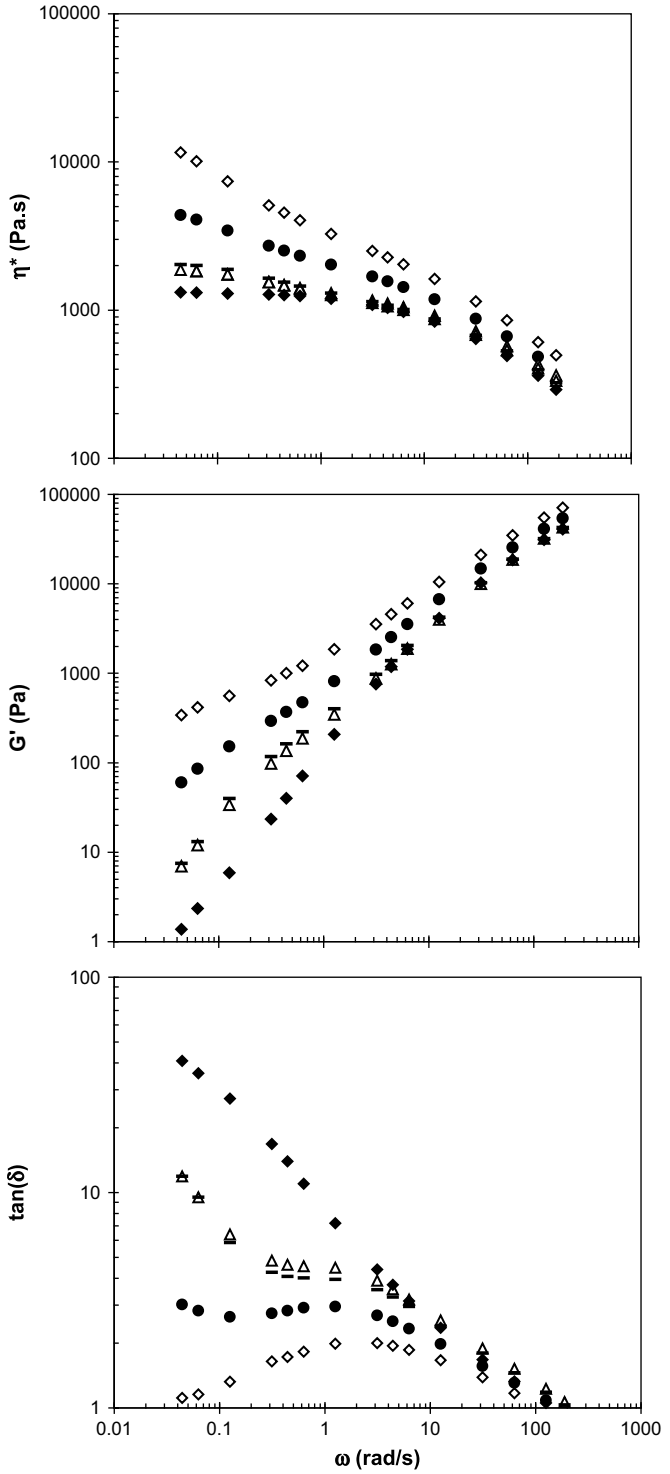

Fig. 5. (a) Complex viscosity (η^*), (b) elastic modulus (G'), and (c) tan δ of the nanocomposites as a function of frequency at 200 °C. Symbols are (◆) PP-g-VTEOS; (–) PP-g-VTEOS/POE; (△) PP-g-VTEOS/POE/oct-SiO_2 2 wt%; (●) PP-g-VTEOS/POE/oct-SiO_2 5 wt%; (◇) PP-g-VTEOS/POE/oct-SiO_2 7 wt%.

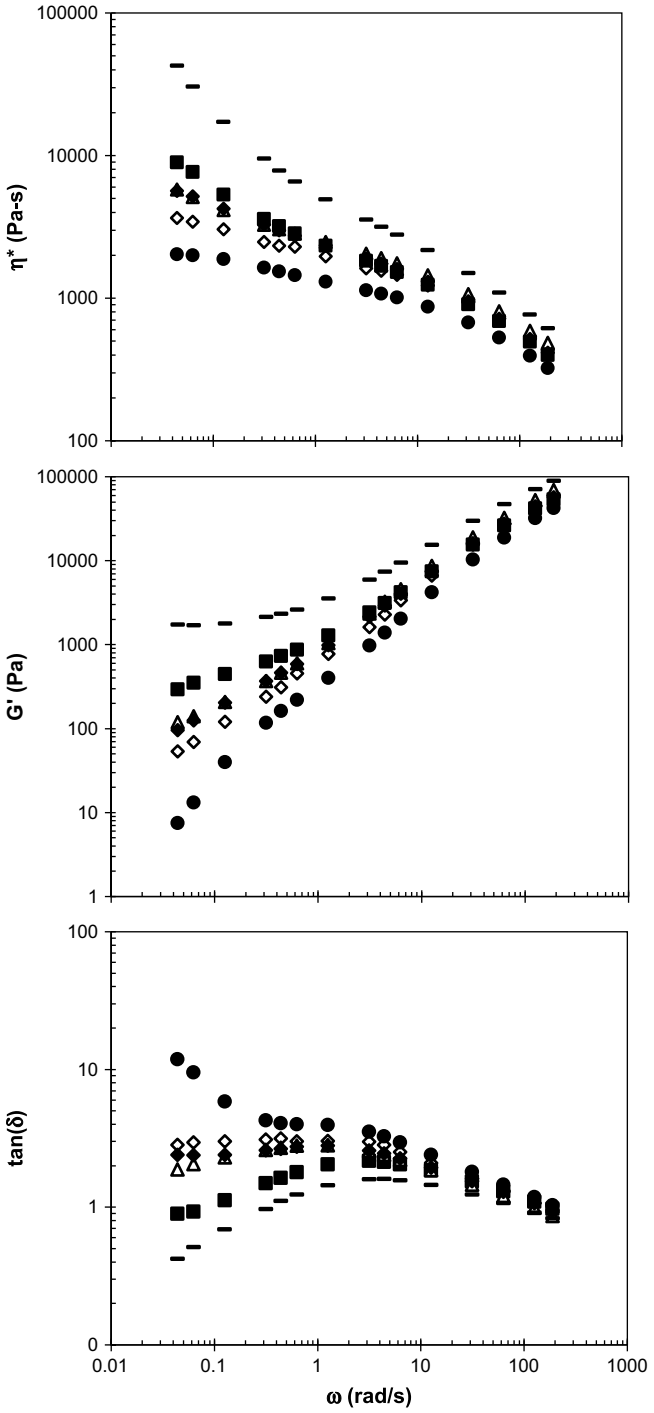

Fig. 6. Complex viscosity (η^*), elastic modulus (G'), and tan δ of the composites as functions of frequency at 200 °C. Symbols are (●) PP-g-VTEOS/POE; (◇) PP-g-VTEOS/POE/SiO_2; (◆) deg-PP/POE/oct-SiO_2; (△) PP-g-VTEOS/POE/hex-SiO_2; (■) PP-g-VTEOS/POE/oct-SiO_2; (–) deg-PP/POE/SiO_2. Silica content is 5 wt%.

efficient load transfer, given that the reinforcement upon silica addition occurs as the load applied during mechanical testing is transferred to the rigid nanoparticles. From Table 3 it becomes obvious that oct-SiO_2, which has the best dispersion as seen on the TEM images (Fig. 2), is the most beneficial filler. In its presence, the Young's and flexural moduli are improved by 33% and 61% respectively at a 5 wt% oct-SiO_2 content compared to PP-g-VTEOS/POE, as shown in Fig. 7. This increase tends to restore the original moduli that the PP matrix had prior to addition of the elastomer. The maximum values are obtained at a 5 wt% silica content in tensile tests and at 7 wt% in flexural tests. A smaller degree of reinforcement is observed for SiO_2 and hex-SiO_2 particles, which exist in a more aggregated state.

On the other hand, the increase in modulus is accompanied by an almost complete loss of the elongation at break, with the

Table 2
Thermal properties of composites containing various amounts and types of nanosilica.

Sample	T_m (°C)	ΔH_f (J/g)	T_c (°C)	ΔH_c (J/g)	Crystallinity (%)
PP	164.9	99.2	118.1	98.9	51.4
PP-g-VTEOS	162.7	102.6	119.4	103.5	53.2
PP-g-VTEOS/POE	161.1	75.0	117.1	75.7	48.6
PP-g-VTEOS/oct-SiO_2 5%	163.6	97.3	118.3	98.4	56.8
PP-g-VTEOS/POE/oct-SiO_2 2%	162.1	83.0	120.6	83.0	55.1
PP-g-VTEOS/POE/oct-SiO_2 5%	162.2	76.9	119.7	79.6	52.4
PP-g-VTEOS/POE/oct-SiO_2 7%	163.2	77.1	121.0	78.1	53.5
PP-g-VTEOS/POE/SiO_2 5%	164.1	88.5	128.5	88.7	60.3
PP-g-VTEOS/POE/hex-SiO_2 5%	163.5	80.0	126.9	80.3	54.5
Deg-PP/POE/oct-SiO_2 5%	160.9	81.9	117.6	82.11	55.9
Deg-PP/POE/SiO_2 5%	162.0	85.7	116.6	87.3	58.4

exception of the oct-SiO_2 containing composites, which maintain some ductility. For this material the most substantial losses in ductility are observed beyond 5 wt% oct-SiO_2 content. This can be explained by the presence of a percolation threshold at contents above 5 wt%, as evidenced by the rheological characterization (Fig. 5). Higher silica contents lead to the formation of agglomerates, which act as stress concentrators. Most importantly, the presence of nanosilica does not compromise impact properties – on the contrary a slight improvement is seen upon the addition of nanofillers, and especially oct-SiO_2 (Fig. 7 and Table 3).

It is worth noting that the addition of oct-SiO_2 to PP-g-VTEOS alone results in significant ductility and toughness reduction (see Table 3). Therefore the improvement seen in the PP-g-VTEOS/POE-based composites can be attributed to the selective localization of the filler, which reinforces the PP-g-VTEOS matrix, while leaving the POE phase intact. The ability of POE to act as an impact modifier for the PP-g-VTEOS matrix remains thus unaffected.

4. Discussion

The physical properties of nanocomposites are largely dependent on the polymer/filler and filler/filler interactions. It is well-established that the reinforcement of the polymer is attributed to the increase in the area of contact between the polymer and the nanofillers, as well as the ability of the polymer and the matrix to form a strong interface, in order to transfer the applied from the matrix to the rigid nanofillers.

In this work, the type of interactions between the silica and the PP matrix depends on the degree of treatment of the silica particles and the functionalization of the matrix. The following mechanisms are prevalent: Firstly, the silanol groups present at the surface of the nanoparticles participate in hydrogen bonding, causing the particles to aggregate when compounded with a hydrophobic matrix like PP. This is the main filler/filler interaction, which causes the formation of micrometer-scale aggregates, the presence of which is unfavourable in terms of mechanical properties.

Secondly, the alkoxysilane functionality engages the hydroxyl groups on the surface of the silica in a hydrolysis reaction, according to Scheme 1, resulting in covalent bonding. This reaction has been previously reported in alumina and silica particles [23,24], as well as glass fiber composites [42–44] and constitutes the predominant mechanism in the composites containing the PP-g-VTEOS matrix. Our results indicate that presence of covalent bonding alone is not sufficient to obtain optimum properties, as evidenced by the results obtained for the composites containing PP-g-VTEOS and unmodified SiO_2. Rather a combination of good dispersion and presence of covalent bonding is needed. This can be achieved by treatment of the nanoparticles with silanes to replace some of the silanol groups by silane groups, thus rendering the particles more hydrophobic, with improved affinity to the polyolefin matrix and a smaller tendency to agglomerate. It should be noted however that since the replacement of silanol groups is only partial, the hydrolysis reaction is still likely to occur. The extent of the interaction with the silane grafts will thus depend on the amount of the free hydroxyl groups remaining after modification. Moreover, the improved dispersion of particles facilitated by the replacement of –OH groups should contribute to a further increase of the surface available for the hydrolysis reaction. The substantial improvement in mechanical properties observed in the oct-SiO_2 containing composites indicates that for this nanosilica grade the extent of particle modification is balanced, so that filler/filler interactions can be reduced enough to prevent particle agglomeration, while leaving a sufficient amount of hydroxyl groups available to form covalent bonds.

The benefits of covalent bonding in terms of strengthening the interface between polymer and filler become apparent when comparing the PP-g-VTEOS/POE/oct-SiO_2 system with its non-functionalized deg-PP/POE/oct-SiO_2 counterpart. Even though the dispersion of oct-SiO_2, as well as that of the dispersed POE phase is not substantially different in the two systems (see Fig. 2 and Table 1) implying that the surface modification of the filler is primarily responsible for its good dispersion, the mechanical properties are substantially enhanced in the presence of covalent bonding (Table 3), which strengthens the interface between polymer and filler. This is further confirmed by the enhancement in rheological properties, which is more pronounced in the PP-g-VTEOS/POE/oct-SiO_2 composite (Fig. 6), compared to the rest of the nanocomposites.

In this work the focus rests on formulating a strategy for impact toughening, which takes advantage of filler-induced matrix reinforcement, while maintaining the impact toughening properties of the polyolefin elastomer. The deformation mechanisms upon addition of a rubbery phase into a thermoplastic matrix have been widely investigated for decades. Stress concentration around the elastomer particles leads to three different mechanisms: multiple shear yielding occurring at the interface matrix/rubber or in the matrix itself, multiple crazing by the formation of crazes either at the vicinity or inside the rubber particles [45], and finally by

Table 3
Mechanical properties of composites containing various amounts and types of nanosilica.

Sample	Young's modulus (MPa)	Tensile stress (MPa)	Elongation at break (%)	Flexural modulus (MPa)	Flexural stress (MPa)	Impact strength (J/m)
PP-g-VTEOS	325.8 ± 48	34.32 ± 1.4	1159 ± 336	1090 ± 34.6	37.9 ± 4	22.4 ± 3.3
PP-g-VTEOS/POE	224.8 ± 13	21.6 ± 1.5	1457 ± 333	573 ± 17	21.9 ± 1.8	39.9 ± 1.5
PP-g-VTEOS/oct-SiO_2 5%	371.1 ± 14	35.9 ± 1.6	38 ± 6.6	1181 ± 27	41.6 ± 0.5	20.4 ± 2.2
PP-g-VTEOS/POE/oct-SiO_2 2%	260.2 ± 9.9	23.8 ± 0.6	713 ± 443	821 ± 22	28.9 ± 0.7	43.0 ± 4.2
PP-g-VTEOS/POE/oct-SiO_2 5%	298.4 ± 15	26.5 ± 0.8	536 ± 241	913 ± 11	30.8 ± 0.4	44.5 ± 3.3
PP-g-VTEOS/POE/oct-SiO_2 7%	278.4 ± 12.4	23.9 ± 0.9	78.4 ± 35	925 ± 17	31 ± 1.2	36.6 ± 2.8
PP-g-VTEOS/POE/SiO_2 5%	259.4 ± 35.9	22.4 ± 0.8	119.8 ± 67	842 ± 13.3	28.9 ± 3.1	40.9 ± 3.2
PP-g-VTEOS/POE/hex-SiO_2 5%	268.1 ± 14.8	22.2 ± 0.8	79.5 ± 29	851 ± 39.8	28.7 ± 0.3	42.9 ± 7.3
Deg-PP/POE/oct-SiO_2 5%	240.4 ± 30.4	23.1 ± 2.1	211.9 ± 117	755 ± 35.0	27.0 ± 1.1	42.7 ± 6.2
Deg-PP/POE/SiO_2 5%	268.6 ± 24.8	20.8 ± 2.7	202.3 ± 160	897 ± 50.7	31.3 ± 1.0	35.6 ± 3.7

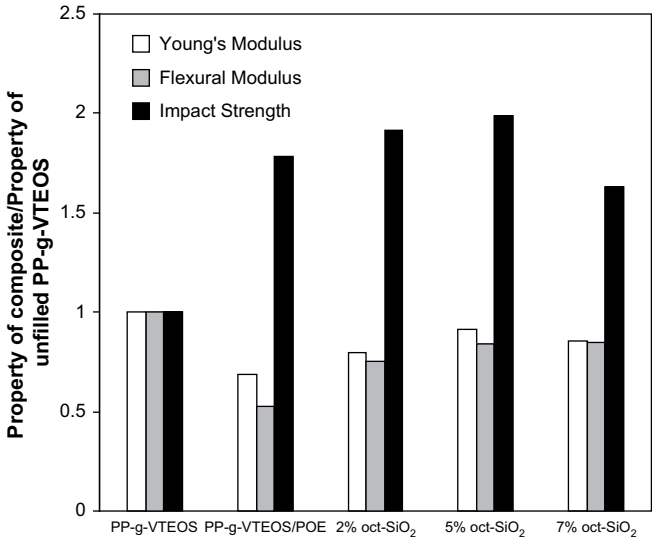

Fig. 7. Effect of oct-SiO_2 loading on the mechanical properties of PP-g-VTEOS. The bars represent the ratio of the physical property of the composite with respect to the property of the unfilled PP-g-VTEOS.

cavitation which often induces stress whitening. The latter mechanism has been observed in our previous work on maleated PP/POE/oct-SiO_2 composites [12].

In order for the POE to act as an efficient impact modifier via the above mechanisms, its beneficial elastomeric properties must remain unaffected by the filler. Therefore ensuring that the filler remains exclusively inside the matrix is crucial in obtaining optimum properties. A calculation of the thermodynamic partitioning of oct-SiO_2 can be done by first estimating the surface tension between two components is made according to the Owens and Wendt equation [46]:

$$\gamma_{AB} = \gamma_A + \gamma_B - 2\sqrt{\gamma_A^d \gamma_B^d} - 2\sqrt{\gamma_A^p \gamma_B^p} \quad (3)$$

where A and B correspond to the two polymer phases (PP and POE respectively); γ is the global surface tension, with γ^p and γ^d respectively being its polar and dispersive contributions so that $\gamma = \gamma^p + \gamma^d$.

The localization of the fillers can then be predicted through the calculation of a wetting coefficient ω:

$$\omega = \frac{\gamma_{SiO_2-B} - \gamma_{SiO_2-A}}{\gamma_{AB}} \quad (4)$$

$\omega < -1$ means that the fillers will tend to go into the POE phase, $-1 < \omega < 1$ implies that the filler will tend to remain at the interface, and $\omega > 1$ indicates that the fillers will tend to go into the PP phase.

Substitution of the surface tension data shown in Table 4, results in a wetting parameter of $\omega = -8.3$ for the unmodified silica, indicating that it has a higher affinity toward the dispersed POE phase. On the contrary a wetting parameter of $\omega = 1.1$ is found at a temperature of 190 °C, indicating that the oct-SiO_2 particles have a higher affinity toward the PP phase, and will thus tend to migrate into the PP matrix upon melt compounding.

We have confirmed these calculations by compounding simultaneously PP, POE and silica, followed by TEM observations. The results were similar, when PP-g-VTEOS was used, indicating that matrix functionalization does not influence substantially the localization of the filler. It is possible therefore when using the modified silica to adopt a one-step compounding procedure, where all components are inserted together in the equipment, and still obtain the desirable partitioning of the filler in the PP matrix, thereby ensuring that a good balance of toughness and stiffness is maintained.

Table 4
Surface tensions of PP, POE and nanosilica at 190 °C.

Material	Surface tension (mJ/m^2)			Reference
	Global	Dispersion	Polar	
PP	21.7	21.2	0.5	[47]
POE	17.5	15.6	1.9	[47]
SiO_2	47	12.9	34.1	[11]
Oct-SiO_2	15.5	15.5	0	[11]

5. Conclusions

Ternary nanocomposites based on a PP-g-VTEOS matrix were prepared via a melt compounding procedure, which resulted in a separated morphology wherein the silica nanoparticles were dispersed in the polypropylene matrix. Surface treatment of the nanosilica with silanes contributed to the fine dispersion of the filler.

Differential scanning calorimetry experiments demonstrated the nucleating effect of the non-treated silica particles via an increase of the crystallization temperature and the degree of crystallinity. However, silane-treated particles did not affect significantly the crystallization process.

Increasing silica concentration significantly changed the rheological behaviour at low frequencies to reach a pseudo-solid like behaviour characterized by a reduced dependency of the complex viscosity and the elastic modulus on the frequency.

The tensile and flexural properties of the composites were improved upon addition of the rigid nanofillers, whereas the impact strength was maintained when the nanosilica was treated with octylsilane. These improvements in properties are attributed to a combination of the localization of finely dispersed fillers in the PP matrix and the presence of covalent bonding due to a hydrolysis reaction between the silanol groups present on the surface of the silica and silane grafts in the polymer. It can be concluded that this approach can generate composites having a good balance of stiffness due to the strengthening of the matrix in the presence of nanosilica, and toughness because of the presence of the unfilled dispersed elastomer phase.

Acknowledgements

This research has been supported by the Natural Sciences and Engineering Research Council of Canada (NSERC). The authors would like to thank Evonic Industries for donating the nanosilica samples used in this work. The contributions of Dr. Khalil El Mabrouk, Charlie Cooney and Doug Holmyard are also greatly appreciated.

References

[1] D'Orazio L, Mancarella C, Martuscelli E, Sticotti G, Massari P. Polymer 1993;34(17):3671–82.
[2] Choudhary V, Varma H, Varma I. Polymer 1991;32(14):2534–40.
[3] Da Silva A, Rocha M, Coutinho F, Bretas R, Scuracchio C. J Appl Polym Sci 1999;72(5):692–704.
[4] Kontopoulou M, Wang W, Gopakumar T, Cheung C. Polymer 2003;44(24):7495–504.
[5] McNally T, McShane P, McNally GM, Murphy WR, Cook C, Miller A. Polymer 2002;43(13):3785–93.
[6] Ma C, Mai Y, Rong M, Ruan W, Zhang M. Comp Sci Techol 2007;67(14):2997–3005.
[7] Jancar J, Dibenedetto A. J Mater Sci 1994;29(17):4651–8.

[8] Long Y, Shanks R. J Appl Polym Sci 1996;61(11):1877–85.
[9] Lee H, Fasulo PD, Rodgers WR, Paul DR. Polymer 2005;46(25):11673–89.
[10] Hanim H, Ahmad Fuad MY, Zarina R, Mohd Ishak A, Hasan A. J Thermoplast Compos Mater 2008;21(2):123–40.
[11] Elias L, Fenouillot F, Majeste JC, Cassagnau P. Polymer 2007;48(20):6029–40.
[12] Liu Y, Kontopoulou M. Polymer 2006;47(22):7731–9.
[13] Liu Y, Kontopoulou M. J Vinyl Add Tech 2007;13(3):147–50.
[14] Yang H, Zhang X, Qu C, Li B, Zhang L, Zhang Q, et al. Polymer 2007;48(3):860–9.
[15] Hasegawa N, Okamoto H, Kawasumi M, Kato M, Tsukigase A, Usuki A. Macromol Mater Eng 2000;280–281:76–9.
[16] Demjen Z, Pukanszky B, Nagy J. Polymer 1999;40(7):1763–73.
[17] Jain S, Goossens J, Van Duin M. Macromol Symp 2006;233:225–34.
[18] Shim J, Joo J, Jung S, Yoon J. J Polym Sci Part B Polym Phys 2007;45(5):607–15.
[19] Bikiaris D, Vassiliou A, Pavlidou E, Karayannidis G. Eur Polym J 2005; 41(9):1965–78.
[20] Rong MZ, Zhang MQ, Ruan WH. Mater Sci Technol 2006;22(7):787–96.
[21] Wu C, Zhang MQ, Rong MZ, Friedrich K. Compos Sci Techol 2002;62(10–11):1327–40.
[22] Rong MZ, Zhang MQ, Zheng Y, Zeng H, Friedrich K. Polymer 2001;42(1):167–83.
[23] Rong MZ, Ji Q, Zhang M, Friedrich K. Eur Polym J 2002;38(8):1573–82.
[24] Rong MZ, Zhang MQ, Pan SL, Lehmann B, Friedrich K. Polym Int 2004;53(7):176–83.
[25] Bikiaris D, Papageorgiou G, Pavlidou E, Vouroutzis N, Palatzoglou P, Karayannidis G. J Appl Polym Sci 2006;100(4):2684–96.
[26] Papageorgiou G, Achilias D, Bikiaris D, Karayannidis G. Thermochim Acta 2005;427(1–2):117–28.
[27] Zhang Q, Archer L. Langmuir 2002;18(26):10435–42.
[28] Aranguren M, Mora E, deGroot J, Macosko C. J Rheol 1992;36(6):1165–82.
[29] Ramier J, Gauthier C, Chazeau L, Stelandre L, Guy L. J Polym Sci Part B Polym Phys 2007;45(3):286–98.
[30] Wu W, Wagner M, Zhongde X. Colloid Polym Sci 2003;281(6):550–5.
[31] Parent JS, Parodi R, Wu W. Polym Eng Sci 2006;46(12):1754–61.
[32] Danusso F, Gianotti G. Eur Polym J 1968;4(1):165–71.
[33] Bartholome C, Beyou E, Bourgeat-Lami E, Cassagneau P, Chaumont P, David L, et al. Polymer 2005;46(23):9965–73.
[34] Ray SS, Pouliot S, Bousmina M, Utracki LA. Polymer 2004;45(25):8403–13.
[35] Voulgaris D, Petridis D. Polymer 2002;43(8):2213–8.
[36] Kontopoulou M, Liu Y, Austin JR, Parent JS. Polymer 2007;48(15):4520–8.
[37] Khatua BB, Lee DJ, Kim HY, Kim JK. Macromolecules 2004;37(7):2454–9.
[38] Austin JR, Kontopoulou M. Polym Eng Sci 2006;46(11):1491–501.
[39] Vermant J, Cioccolo G, Golapan Nair K, Moldenaers P. Rheol Acta 2004; 43(5):529–38.
[40] Cassagnau P. Polymer 2008;49(9):2183–97.
[41] Mekhilef J, Carreau PJ, Favis BD, Martin P, Ouhlal A. J Polym Sci Part B Polym Phys 2000;38(10):1359–68.
[42] Zhou X, Dai G, Guo W, Lin Q. J Appl Polym Sci 2000;76:1359–65.
[43] Bikiaris D, Matzinos P, Larena A, Flaris V, Panayiotou C. J Appl Polym Sci 2001;81(3):701–9.
[44] Qiu W, Mai K, Zeng H. J Appl Polym Sci 1999;71(10):1537–42.
[45] Liang JZ, Li RKY. J Appl Polym Sci 2000;77(2):409–17.
[46] Owens Daniel K, Wendt RC. J Appl Polym Sci 1969;13(8):1741–7.
[47] Ma C, Zhang M, Rong M. J Appl Polym Sci 2007;103(3):1578–84.